

μ-Hydroxo-μ-phenolato Dinuclear Zinc(II) and Nickel(II) Complexes Derived from Dinucleating Compartmental Ligands of "End-off" Type: Synthesis, Structures, and Properties

Kanako Matsufuji, Hitomi Shiraishi, Yuji Miyasato, Takuya Shiga, Masaaki Ohba,† Takushi Yokoyama, and Hisashi Ōkawa*

Department of Chemistry, Faculty of Science, Kyushu University, Hakozaki 6-10-1, Higashi-ku, Fukuoka 812-8581

Received October 25, 2004; E-mail: okawascc@mbox.nc.kyushu-u.ac.jp

Some dinucleating compartmental ligands of "end-off" type, 2,6-bis{*N*-[(2-dimethylamino)ethyl]iminomethyl}-4-methylphenol (HL^1), 2,6-bis{*N*-(2-pyridylethyl)iminomethyl}-4-methylphenol (HL^2), and 2,6-bis{*N*,*N*-di(2-pyridylmethyl)aminomethyl}-4-methylphenol (HL^3), have afforded the following dinuclear Zn(II) and Ni(II) complexes: $[Zn_2(L^1)(OH)(py)_2](ClO_4)_2$ (**1**), $[Zn_2(L^2)(OH)(py)_3](ClO_4)_2$ (**2**), $[Zn_2(L^3)(OH)](ClO_4)_2$ (**3**), $[Ni_2(L^1)(OH)(py)_2](ClO_4)_2$ (**4**), and $[Ni_2(L^2)(OH)(py)_4](ClO_4)_2$ (**5**). X-ray crystallographic studies for **1**·Pr^2OH, **2**·0.5Pr^2OH, **3**·MeCN, **4**·py, and **5** indicate that they have a dinuclear core doubly bridged by the endogenous phenolic oxygen of each compartmental ligand and by exogenous hydroxide oxygen. Physicochemical properties of **1**–**5** are studied.

Bimetallic cores exist at the active sites of many metalloenzymes and play an essential role in biological systems.[1] Dinuclear Zn cores are found at the active site of hydroxylases such as *Alkaline phosphatase*,[2] *Phospholipase C*,[3] *P1 nuclease*,[4] *phosphotriesterase*,[5] and *Leucine amino peptidase*.[6] Moreover, dinuclear FeZn,[7,8] FeMn,[9] MnMn,[10–12] and NiNi[13] cores are recognized for other hydroxylases. It is supposed that these enzymes employ a dinuclear core to facilitate the concerted binding of the substrate on one metal center and the nucleophilic attack of water or hydroxide on the other metal center. Recent X-ray crystallographic studies for *Phospholipase C*,[3] *P1 nuclease*,[4] *Human protein nuclease 1*,[9] *Protein phosphatase 2C*,[10,11] and *Arginase*[12] have clarified the presence of an aqua bridge between a pair of metal ions. In urease from *Klebsiella aerogenes*[13] a water molecule bonded to one Ni center is situated close to another Ni center, suggesting that aqua-bridged dinuclear nickel core can be involved in physiological condition. Such an aqua bridge is rare in synthetic metal complexes, whereas a hydroxide bridge often occurs in dinuclear and polynuclear metal complexes. Thus, we are interested in the hydrolytic activity of μ-hydroxo dinuclear metal complexes with relevance to aqua-bridged bimetallic hydroxylases.

Dinucleating compartmental ligands of "end-off" type have often been used for modeling bimetallic biosites. In this work some dinucleating compartmental ligands of "end-off" type, 2,6-bis{*N*-[(2-dimethylamino)ethyl]iminomethyl}-4-methylphenol (HL^1), 2,6-bis{*N*-[(2-pyridyl)ethyl]iminomethyl}-4-methylphenol (HL^2), and 2,6-bis[*N*,*N*-di(2-pyridylmethyl)aminomethyl]-4-methylphenol (HL^3) (Fig. 1), are used to produce the following dinuclear Zn(II) and Ni(II) complexes: $[Zn_2(L^1)(OH)(py)_2](ClO_4)_2$ (**1**), $[Zn_2(L^2)(OH)(py)_3](ClO_4)_2$ (**2**), $[Zn_2(L^3)(OH)](ClO_4)_2$ (**3**), $[Ni_2(L^1)(OH)(py)_2](ClO_4)_2$ (**4**), and $[Ni_2(L^2)(OH)(py)_4](ClO_4)_2$ (**5**). X-ray crystallographic studies for **1**·Pr^2OH (Pr^2OH = 2-propanol), **2**·0.5Pr^2OH, **3**·MeCN, **4**·py, and **5** indicate a dinuclear core doubly bridged by the endogenous phenolic oxygen of the respective compartmental ligand and by the hydroxide oxygen. Physicochemical properties of **1**–**5** are reported in this paper.

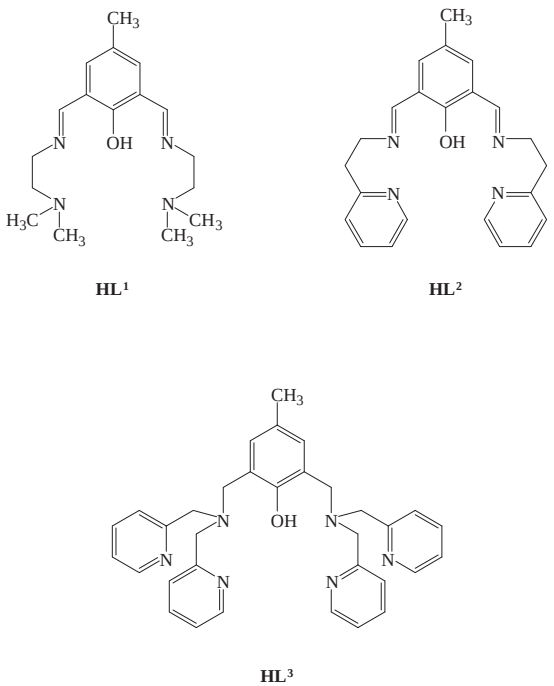

Fig. 1. Chemical structures of HL^1–HL^3.

Experimental

Physical Measurements. Elemental analyses of carbon, hy-

† Present address: Graduate School of Engineering, Department of Synthetic Chemistry and Biological Chemistry, Kyoto University, Katsura, Nishikyo-ku, Kyoto 615-8510

Published on the web May 6, 2005; DOI 10.1246/bcsj.78.851

drogen, and nitrogen were obtained at The Service Center of Elemental Analysis of Kyushu University. Metal analyses were obtained on a Shimadzu AA-680 Atomic Absorption/Flame Emission Spectrophotometer. Infrared spectra were recorded using a KBr disk on a PERKIN ELEMER Spectrum BX FT-IR system. Electronic absorption spectra were recorded on a Shimadzu UV-3100PC spectrophotometer. Molar conductances in DMSO were measured using a DKK AOL-10 conductivity meter at room temperature. Magnetic susceptibilities of powdered samples were measured on a Quantum Design MPMS XL SQUID susceptometer in the temperature range of 2–300 K.

Synthesis. 2,6-Diformyl-4-methylphenol and the ligands HL^3 were prepared by the literature methods.[14,15] Other chemicals were purchased from commercial sources and were used without further purification.

$[Zn_2(L^1)(OH)(py)_2](ClO_4)_2$ (1). The ligand HL^1 was prepared in situ by the reaction of 2,6-diformyl-4-methylphenol (0.083 g, 0.5 mmol) and *N*,*N*-dimethylethylenediamine (0.098 g, 1.0 mmol) in hot pyridine (10 cm^3). To this solution were added zinc(II) perchlorate hexahydrate (0.426 g, 1.0 mmol) and triethylamine (0.101 g, 1.0 mmol), the mixture was stirred for 30 min and diffused with 2-propanol to give yellow microcrystals. Yield: 0.397 g (92%). Anal. Calcd for $C_{27}H_{38}Cl_2N_6O_{10}Zn_2$: C, 41.49; H, 5.34; N, 9.68; Zn, 15.06%. Found: C, 41.62; H, 5.34; N, 9.83; Zn, 15.18%. Selected FT-IR data [ν/cm^{-1}] using a KBr disk: 3599, 1647, 1606, 1550, 1448, 1104, 624. Molar conductance [Λ_M/S cm^2 mol^{-1}]: 55 in DMSO. UV–vis [λ_{max}/nm (ε/M^{-1} cm^{-1})]: 390 (10600) in DMSO.

Single crystals of $[Zn_2(L^1)(OH)(py)_2](ClO_4)_2 \cdot Pr^2OH$ (**1**·Pr^2OH) suitable for X-ray structural analysis were grown when a pyridine solution of **1** was diffused with 2-propanol.

$[Zn_2(L^2)(OH)(py)_3](ClO_4)_2$ (2). The ligand HL^2 was prepared in situ by the reaction of 2,6-diformyl-4-methylphenol (0.082 g, 0.5 mmol) and 2-(2-pyridyl)ethylamine (0.122 g, 1.0 mmol) in hot pyridine (10 cm^3). To this solution were added zinc(II) perchlorate hexahydrate (0.372 g, 1.0 mmol) and triethylamine (0.101 g, 1.0 mmol), and the mixture was stirred for 30 min and diffused with 2-propanol to form yellow crystals. Yield: 0.261 g (48%). Anal. Calcd for $C_{38}H_{39}Cl_2N_7O_{10}Zn_2$: C, 47.77; H, 4.11; Cl, 7.42; N, 10.26; O, 16.75; Zn, 13.69%. Found: C, 47.87; H, 4.23; N, 10.22; Zn, 13.25%. Selected IR data [ν/cm^{-1}] using a KBr disk: 3620, 1640, 1605, 1552, 1484, 1447, 1098, 624. Molar conductance [Λ_M/S cm^2 mol^{-1}]: 61 in DMSO. UV–vis [λ_{max}/nm (ε/M^{-1} cm^{-1})]: 391 (11600) in DMSO.

Single crystals of **2**·0.5Pr^2OH were grown when a pyridine solution of **2** was diffused with 2-propanol.

$[Zn_2(L^3)(OH)](ClO_4)_2$ (3). A solution of zinc(II) perchlorate hexahydrate (0.372 g, 1.0 mmol) in hot acetonitrile (5 cm^3) was added to a solution of HL^3 (0.265 g, 0.5 mmol) in hot acetonitrile (10 cm^3), and the mixture was stirred for 30 min. To this solution was added triethylamine (0.101 g, 1.0 mmol), and the mixture was diffused with diethyl ether to give colorless crystals of $[Zn_2(L^3)(OH)](ClO_4)_2 \cdot MeCN$ (**3**·MeCN). It was dried in vacuo to obtain $[Zn_2(L^3)(OH)](ClO_4)_2$ (**3**). Yield: 0.425 g (96%). Anal. Calcd for $C_{33}H_{34}Cl_2N_6O_{10}Zn_2$: C, 45.23; H, 3.91; N, 9.59; Zn, 14.92%. Found: C, 44.84; H, 3.84; N, 9.48; Zn, 14.33%. Selected IR data [ν/cm^{-1}] using a KBr disk: 3611, 1610, 1576, 1478, 1444, 1085, 623. Molar conductance [Λ_M/S cm^2 mol^{-1}]: 55 In DMSO. UV–vis [λ_{max}/nm (ε/M^{-1} cm^{-1})]: 307 (3200) in DMSO.

$[Ni_2(L^1)(OH)(py)_2](ClO_4)_2$ (4). This complex was obtained as green crystals in a way similar to that for **1** except for the use of nickel(II) perchlorate hexahydrate (0.375 g, 1.0 mmol). Yield: 0.324 g (78%). Anal. Calcd for $C_{27}H_{38}Cl_2N_6Ni_2O_{10}$: C, 40.79; H, 4.82; N, 10.57; Ni, 14.77%. Found: C, 41.03; H, 4.89; N, 10.87; Ni, 14.85%. Selected IR data [ν/cm^{-1}] using a KBr disk: 3604, 1651, 1604, 1549, 1446, 1119, 1078, 624. Molar conductance [Λ_M/S cm^2 mol^{-1}]: 56 in DMSO. UV–vis [λ_{max}/nm (ε/M^{-1} cm^{-1})]: 402 (7900), 624 (30), 920 (22), and 1400 (15) in pyridine; 409 (5700), ~490sh (ca. 300), 900 (12), and ~1350 (5) in DMSO.

Single crystals of $[Ni_2(L^1)(OH)(py)_2](ClO_4)_2 \cdot py$ (**4**·py) suitable for X-ray crystallography were grown when a pyridine solution of **4** was diffused with 2-propanol.

$[Ni_2(L^1)(OH)(H_2O)](ClO_4)_2$ (4′). Crystals of **4** were heated at 130 °C for 24 h to obtain a red powder. It was dissolved in dichloromethane and the solution was diffused with diethyl ether in open air to obtain red crystals. Yield: 82%. Anal. Calcd for $C_{17}H_{30}Cl_2N_4Ni_2O_{11}$: C, 31.19; H, 4.62; N, 8.56; Ni, 17.93%. Found: C, 31.18; H, 4.67; N, 8.66; Ni, 18.17%. Selected IR data [ν/cm^{-1}] using a KBr disk: 3573, 1653, 1627, 1556, 1462, 1089, 627. UV–vis [λ_{max}/nm (ε/M^{-1} cm^{-1})]: 403 (14300), 583 (16), 990 (25) in pyridine; 409 (~300), 905 (12), 1350 (5) in DMSO.

$[Ni_2(L^2)(OH)(py)_4](ClO_4)_2$ (5). This was obtained as green crystals in a way similar to that for **2**, using nickel(II) perchlorate hexahydrate (0.369 g, 1.0 mmol) instead of zinc(II) perchlorate hexahydrate. Yield: 57%. Anal. Calcd for $C_{43}H_{44}Cl_2N_8Ni_2O_{10}$: C, 50.58; H, 4.34; N, 10.97; Ni, 11.50%. Found: C, 50.62; H, 4.39; N, 10.96; Ni, 11.53%. Selected IR data [ν/cm^{-1}] using a KBr disk: 3644, 1638, 1602, 1550, 1488, 1445, 1095, 623. Molar conductance [Λ_M/S cm^2 mol^{-1}]: 58 in DMSO. UV–vis [λ_{max}/nm (ε/M^{-1} cm^{-1})]: 403 (7200), 583 (16), and 990 (25) in pyridine; 400 (8300), 593 (23), 905 (12), and 1350 (10) in DMSO.

X-ray Crystallography. Each single crystal of **1**·Pr^2OH, **3**·MeCN, and **4**·py was mounted on a glass fiber. Measurements were made on a Rigaku RAXIS-RAPID Imaging Plate diffractometer using graphite monochromated Mo Kα radiation at -120 ± 1 °C for **1**·Pr^2OH and **4**·py and at -60 ± 1 °C for **3**·MeCN. Data were processed by the PROCESS-AUTO program package. Each single crystal of **2**·0.5Pr^2OH and **5** was mounted on a glass fiber and used for measurements on a Rigaku AFC7R diffractometer with graphite monochromated Mo Kα radiation and a rotating anode generator. The data were collected at 23 ± 1 °C using the ω-2θ scan technique.

The structures were solved by direct method and expanded using Fourier technique. The non-hydrogen atoms were refined anisotropically. Hydrogen atoms were included but not refined. All calculations were performed using the teXsan crystallographic software package of Molecular Structure Corporation.[16] Pertinent crystallographic parameters are given in Table 1.

Crystallographic data have been deposited with Cambridge Crystallographic Data Center as supplementary publication no. CCDC 211807–211811. Copies of the data can be obtained free of charge via www.ccdc.cam.ac.uk/conts/retrieving.html (or from the Cambridge Crystallographic Data Center, 12, Union Road, Cambridge, CB2 1EZ, UK; Fax: +44 1223 336033; ordeposit@ccdc.cam..ac.uk).

Results and Discussion

Preparation. The μ-hydroxo-zinc(II) and nickel(II) complexes of $(L^1)^-$ and $(L^2)^-$ were prepared by the reaction of the respective ligand with $M(ClO_4)_2 \cdot 6H_2O$ (M = Zn, Ni) in pyridine. The ligand $(L^1)^-$ afforded bis(pyridine) complexes,

Table 1. Crystallographic Data of **1**·Pr^2OH, **2**·0.5Pr^2OH, **3**·MeCN, **4**·py, and **5**

	1·Pr^2OH	**2**·0.5Pr^2OH	**3**·MeCN	**4**·py	**5**
Formula	$C_{30}Cl_2H_{46}N_6O_{11}Zn_2$	$C_{39.5}Cl_2H_{45}N_7O_{10.5}Zn_2$	$C_{35}Cl_2H_{39}N_7O_{11}Zn_2$	$C_{32}Cl_2H_{43}N_7Ni_2O_{10}$	$C_{43}Cl_2H_{44}N_8Ni_2O_{10}$
Formula weight	868.39	987.51	935.41	874.03	1021.17
Crystal system	orthorhombic	triclinic	triclinic	monoclinic	triclinic
Space group	*Pbca*	$P\bar{1}$	$P\bar{1}$	*C*2/*c*	$P\bar{1}$
a/Å	14.6637(3)	11.382(2)	10.0191(6)	15.7931(4)	11.12(4)
b/Å	16.9657(4)	19.530(2)	12.0393(6)	15.2289(4)	20.35(4)
c/Å	29.6924(5)	10.212(1)	17.929(1)	31.3890(8)	10.92(3)
α/°	90.00	92.04(1)	74.017(3)		94.8(2)
β/°	90.00	103.92(1)	81.975(4)	100.120(2)	115.1(2)
γ/°	90.00	97.77(1)	87.013(2)		84.5(2)
V/Å^3	7386.9(3)	2177.6(6)	2058.4(2)	7432.0(3)	2227(10)
Z value	8	2	2	8	2
D_{calcd}/g cm^{-3}	1.562	1.506	1.509	1.491	1.523
μ(Mo Kα)/cm^{-1}	15.08	12.89	13.60	12.18	10.33
No. observations	8415	5758	8930	7835	7381
R	0.083	0.056	0.095	0.077	0.051
R_w	0.087	0.076	0/199	0.170	0.067

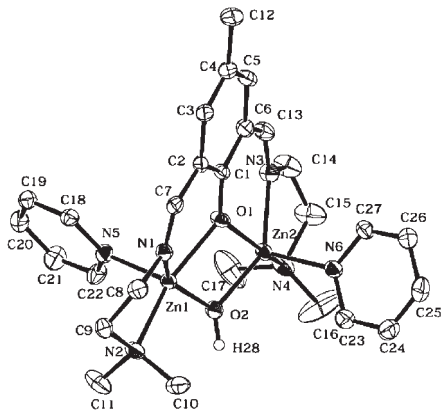

Fig. 2. An ORTEP drawing of $[Zn_2(L^1)(OH)(py)_2](ClO_4)_2$·$Pr^2OH$ (**1**·Pr^2OH).

$[M_2(L^1)(OH)(py)_2](ClO_4)_2$ (M = Zn (**1**) and Ni (**4**)), whereas $(L^2)^-$ afforded tris(pyridine) and tetrakis(pyridine) complexes, $[Zn_2(L^2)(OH)(py)_3](ClO_4)_2$ (**2**) and $[Ni_2(L^2)(OH)(py)_4](ClO_4)_2$ (**5**), respectively. Green **4** turned red on heating at 130 °C and the crystallization of the red compound from dichloromethane/diethyl ether afforded $[Ni_2(L^1)(OH)(H_2O)](ClO_4)_2$ (**4′**). This proved to be a mixed-spin Ni($S = 1$)–Ni($S = 0$) complex as discussed later.

$[Zn_2(L^3)(OH)](ClO_4)_2$ (**3**) was obtained in a tolerable yield when HL^3 and $Zn(ClO_4)_2 \cdot 6H_2O$ were reacted in acetonitrile in the presence of triethylamine. The corresponding nickel complex of HL^3 could not be prepared by a similar method.

Crystal Structures. $Zn_2(L^1)(OH)(py)_2](ClO_4)_2$·$Pr^2OH$ (1·Pr^2OH): An ORTEP drawing is shown in Fig. 2 together with the atom numbering scheme. Selected bond distances and angles are given in Table 2.

The $[Zn_2(L^1)(OH)(py)_2]^{2+}$ cation has a dinuclear core bridged by hydroxide and phenolate ions in a Zn(1)···Zn(2) interatomic separation of 3.116 Å. Each Zn has a five-coordinate geometry together with one pyridine molecule. The geometry about Zn(1) can be regarded as a distorted square-pyramid with the phenolic oxygen O(1), the hydroxide oxygen O(2), the imine nitrogen N(1) and the amine nitrogen N(2) on the equatorial base and the pyridine nitrogen N(5) at the apex. The parameter τ[18] that discriminates square-pyramid ($\tau = 0$) and trigonal-bipyramid ($\tau = 1$) is 0.11. The geometry about Zn(2) is also square-pyramidal (τ: 0.09) with the pyridine nitrogen N(6) at the apex. The Zn-to-donor bond distances fall in the range of 1.946–2.174 Å. The two pyridine molecules are situated trans with respect to the mean molecular plane.

Table 2. Selected Bond Distances and Angles of **1**·Pr^2OH

Bond distances/Å			
Zn(1)–O(1)	2.073(3)	Zn(1)–O(2)	1.946(3)
Zn(1)–N(1)	2.082(3)	Zn(1)–N(2)	2.141(3)
Zn(1)–N(5)	2.082(3)	Zn(2)–O(1)	2.099(3)
Zn(2)–O(2)	1.953(3)	Zn(2)–N(3)	2.068(3)
Zn(2)–N(4)	2.174(3)	Zn(2)–N(6)	2.074(3)
Zn(1)···Zn(2)	3.166(3)		
Bond angles/°			
Zn(1)–O(1)–Zn(2)	97.8(1)	Zn(1)–O(2)–Zn(2)	105.6(1)
O(1)–Zn(1)–O(2)	78.2(1)	O(1)–Zn(1)–N(1)	83.6(1)
O(1)–Zn(1)–N(2)	145.6(1)	O(1)–Zn(1)–N(5)	107.9(1)
O(2)–Zn(1)–N(1)	152.4(1)	O(2)–Zn(1)–N(2)	103.1(1)
O(2)–Zn(1)–N(5)	105.1(1)	N(1)–Zn(1)–N(2)	80.6(1)
N(1)–Zn(1)–N(5)	100.1(1)	N(2)–Zn(1)–N(5)	104.9(1)
O(1)–Zn(2)–O(2)	77.4(1)	O(1)–Zn(2)–N(3)	84.0(1)
O(1)–Zn(2)–N(4)	151.8(1)	O(1)–Zn(2)–N(6)	100.2(1)
O(2)–Zn(2)–N(3)	146.3(1)	O(2)–Zn(2)–N(4)	102.6(1)
O(2)–Zn(2)–N(6)	107.1(1)	N(3)–Zn(2)–N(4)	81.2(1)
N(3)–Zn(2)–N(6)	103.7(1)	N(4)–Zn(2)–N(6)	106.6(1)

$[Zn_2(L^2)(OH)(py)_3](ClO_4)_2 \cdot 0.5Pr^2OH$ (2·0.5Pr^2OH): ORTEP drawings are shown in Fig. 3 together with the atom numbering scheme. Selected bond distances and angles are given in Table 3.

The $[Zn_2(L^2)(OH)(py)_3]^{2+}$ cation has a μ-hydroxo-μ-phe-

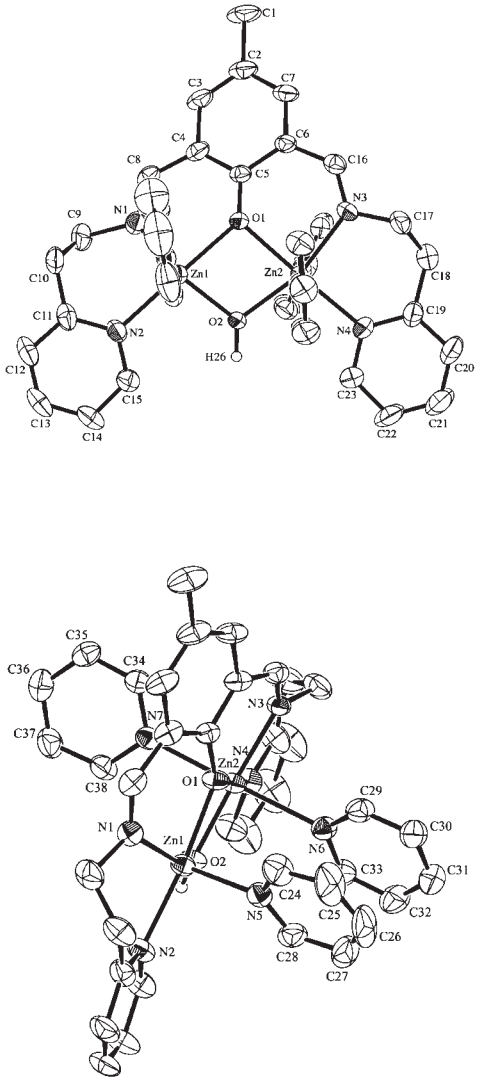

Fig. 3. ORTEP drawings of $[Zn_2(L^2)(OH)(py)_3](ClO_4)_2 \cdot 0.5Pr^2OH$ (**2**·0.5Pr^{2}OH).

nolato-dizinc(II) core in a Zn(1)···Zn(2) interatomic separation of 3.139 Å. Zn(1) has a five-coordinate geometry with further coordination of one pyridine molecule whereas Zn(2) has a six-coordinate geometry together with two pyridine molecules. The geometry about Zn(1) is intermediate between square-pyramid and trigonal-bipyramid (τ: 0.58). The Zn(1)-to-donor bond distances fall in the range of 1.951–2.179 Å. The Zn(2)-to-donor bond distances fall in the range of 2.008–2.339 Å. It must be pointed out that the Zn(2)–N(pyridine) bond distances are quite elongated (2.339(5) and 2.259(5) Å). The pyridine molecule bonded to Zn(2) and one pyridine molecule bonded to Zn(1) are weakly stacked in an average ring–ring separation of 3.82 Å.

$[Zn_2(L^3)(OH)](ClO_4)_2 \cdot$MeCN (3·MeCN): An ORTEP[17] drawing is shown in Fig. 4 together with the atom numbering scheme. Selected bond distances and angles are given in Table 4.

The asymmetric unit consists of one $[Zn_2(L^3)(OH)]^{2+}$ cation, two perchlorate anions and one acetonitrile molecule. The cation has a μ-hydroxo-μ-phenolato-dizinc(II) core in a

Table 3. Selected Bond Distances and Angles of **2**·0.5Pr^{2}OH

Bond distances/Å			
Zn(1)–O(1)	2.106(4)	Zn(1)–O(2)	1.951(4)
Zn(1)–N(1)	2.046(5)	Zn(1)–N(2)	2.179(5)
Zn(1)–N(5)	2.098(5)	Zn(2)–O(1)	2.105(4)
Zn(2)–O(2)	2.008(3)	Zn(2)–N(3)	2.091(4)
Zn(2)–N(4)	2.164(5)	Zn(2)–N(6)	2.339(5)
Zn(2)–N(7)	2.259(5)	Zn(1)···Zn(2)	3.139(5)
Bond angles/°			
Zn(1)–O(1)–Zn(2)	96.4(2)	Zn(1)–O(2)–Zn(2)	104.9(2)
O(1)–Zn(1)–O(2)	79.6(1)	O(1)–Zn(1)–N(1)	86.1(2)
O(1)–Zn(1)–N(2)	174.2(2)	O(1)–Zn(1)–N(5)	92.3(2)
O(2)–Zn(1)–N(1)	139.6(2)	O(2)–Zn(1)–N(2)	98.8(2)
O(2)–Zn(1)–N(5)	111.3(2)	N(1)–Zn(1)–N(2)	91.7(2)
N(1)–Zn(1)–N(5)	106.8(2)	N(2)–Zn(1)–N(5)	93.4(2)
O(1)–Zn(2)–O(2)	78.4(1)	O(1)–Zn(2)–N(3)	85.0(2)
O(1)–Zn(2)–N(4)	176.4(2)	O(1)–Zn(2)–N(6)	93.9(2)
O(1)–Zn(2)–N(7)	89.4(2)	O(2)–Zn(2)–N(3)	162.4(2)
O(2)–Zn(2)–N(4)	103.5(2)	O(2)–Zn(2)–N(6)	90.2(2)
O(2)–Zn(2)–N(7)	91.3(2)	N(3)–Zn(2)–N(4)	93.5(2)
N(3)–Zn(2)–N(6)	85.3(2)	N(3)–Zn(2)–N(7)	94.1(2)
N(4)–Zn(2)–N(6)	89.2(2)	N(4)–Zn(2)–N(7)	87.5(2)
N(6)–Zn(2)–N(7)	176.7(2)		

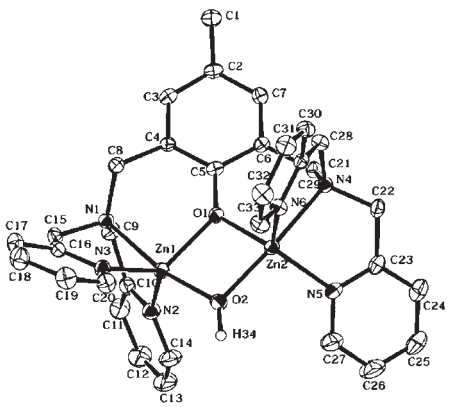

Fig. 4. An ORTEP drawing of $[Zn_2(L^3)(OH)](ClO_4)_2 \cdot$MeCN (**3**·MeCN).

Zn(1)···Zn(2) separation of 3.042 Å. Both Zn(1) and Zn(2) have a five-coordinate geometry. The parameter τ is 0.70 for Zn(1) and 0.63 for Zn(2). Thus, the geometry about each metal is close to trigonal-bipyramid. The Zn(1)–O(2) and Zn(2)–O(2) bond distances (1.943(3) and 1.971(3) Å, respectively) are significantly short relative to the Zn(1)–O(1) and Zn(2)–O(1) bond distances (2.033(3) and 2.030(3) Å, respectively). The Zn-to-N bond distances fall in the range of 2.035(4)–2.208(4) Å.

$[Ni_2(L^1)(OH)(py)_2](ClO_4)_2 \cdot$py (4·py): An ORTEP drawing of **4**·py is shown in Fig. 5, together with the atom numbering scheme. Selected bond distances and angles are given in Table 5.

The structure of the cation resembles that of **1**·Pr^{i}OH. The Ni(1)···Ni(2) interatomic separation is 3.069 Å. Ni(1) and Ni(2) each have a five-coordinate geometry together with

Table 4. Selected Bond Distances and Angles of **3**·MeCN

Bond distances/Å			
Zn(1)–O(1)	2.033(3)	Zn(1)–O(2)	1.943(3)
Zn(1)–N(1)	2.186(4)	Zn(1)–N(2)	2.062(4)
Zn(1)–N(3)	2.056(4)	Zn(2)–O(1)	2.030(3)
Zn(2)–O(2)	1.971(3)	Zn(2)–N(4)	2.208(4)
Zn(2)–N(5)	2.035(4)	Zn(2)–N(6)	2.043(4)
Zn(1)···Zn(2)	3.042(4)		
Bond angles/°			
Zn(1)–O(1)–Zn(2)	96.9(2)	Zn(1)–O(2)–Zn(2)	102.0(2)
O(1)–Zn(1)–O(2)	80.6(1)	O(1)–Zn(1)–N(1)	88.3(1)
O(1)–Zn(1)–N(2)	108.7(2)	O(1)–Zn(1)–N(3)	126.5(2)
O(2)–Zn(1)–N(1)	168.2(1)	O(2)–Zn(1)–N(2)	107.8(2)
O(2)–Zn(1)–N(3)	103.9(2)	N(1)–Zn(1)–N(2)	79.2(2)
N(1)–Zn(1)–N(3)	79.7(1)	N(2)–Zn(1)–N(3)	119.6(2)
O(1)–Zn(2)–O(2)	80.0(1)	O(1)–Zn(2)–N(4)	88.8(1)
O(1)–Zn(2)–N(5)	127.5(2)	O(1)–Zn(2)–N(6)	110.5(2)
O(2)–Zn(2)–N(4)	165.3(1)	O(2)–Zn(2)–N(5)	99.1(2)
O(2)–Zn(2)–N(6)	112.8(2)	N(4)–Zn(2)–N(5)	80.2(2)
N(4)–Zn(2)–N(6)	80.0(1)	N(5)–Zn(2)–N(6)	117.6(2)

Table 5. Selected Bond Distances and Angles of **4**·py

Bond distances/Å			
Ni(1)–O(1)	2.014(2)	Ni(1)–O(2)	1.972(2)
Ni(1)–N(1)	2.008(3)	Ni(1)–N(2)	2.095(3)
Ni(1)–N(5)	2.046(3)	Ni(2)–O(1)	2.020(2)
Ni(2)–O(2)	1.970(2)	Ni(2)–N(3)	2.019(3)
Ni(2)–N(4)	2.102(3)	Ni(2)–N(6)	2.037(3)
Ni(1)···Ni(2)	3.069(3)		
Bond angles/°			
Ni(1)–O(1)–Ni(2)	99.2(2)	Ni(1)–O(2)–Ni(2)	102.4(2)
O(1)–Ni(1)–O(2)	79.2(1)	O(1)–Ni(1)–N(1)	88.0(1)
O(1)–Ni(1)–N(2)	163.9(1)	O(1)–Ni(1)–N(5)	97.1(1)
O(2)–Ni(1)–N(1)	155.9(1)	O(2)–Ni(1)–N(2)	103.3(1)
O(2)–Ni(1)–N(5)	98.2(1)	N(1)–Ni(1)–N(2)	83.7(1)
N(1)–Ni(1)–N(5)	103.6(1)	N(2)–Ni(1)–N(5)	98.3(1)
O(1)–Ni(2)–O(2)	79.1(1)	O(1)–Ni(2)–N(3)	87.5(1)
O(1)–Ni(2)–N(4)	160.9(1)	O(1)–Ni(2)–N(6)	97.2(1)
O(2)–Ni(2)–N(3)	153.8(1)	O(2)–Ni(2)–N(4)	102.2(1)
O(2)–Ni(2)–N(6)	101.4(1)	N(3)–Ni(2)–N(4)	83.5(1)
N(3)–Ni(2)–N(6)	102.5(1)	N(4)–Ni(2)–N(6)	101.2(1)

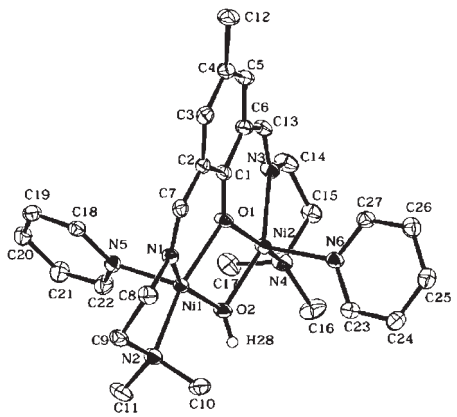

Fig. 5. An ORTEP drawing of $[Ni_2(L^1)(OH)(py)_2](ClO_4)_2$·py (**4**·py).

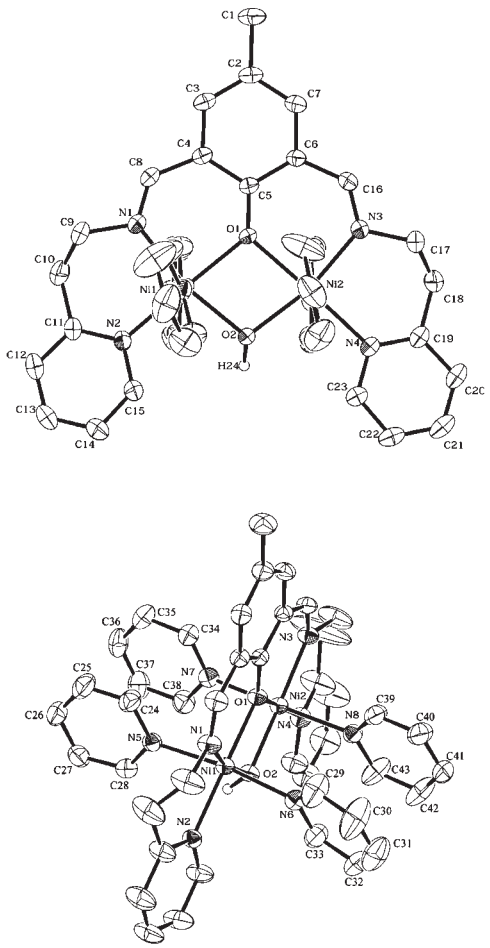

Fig. 6. ORTEP drawings of $[Ni_2(L^2)(OH)(py)_4](ClO_4)_2$ (**5**).

one pyridine molecule. The geometry about each Ni is regarded as a square-pyramid with the pyridine nitrogen at the apex; the τ value is 0.13 for Ni(1) and 0.12 for Ni(2). The Ni-to-donor bond distances fall in the range of 1.970–2.102 Å. The Ni(1)–O(1)–Ni(2) and Ni(1)–O(2)–Ni(2) angles are 99.2° and 102.4°, respectively. The pyridine molecule on Ni(1) and that on Ni(2) are situated trans with respect to the mean molecular plane.

$[Ni_2(L^2)(OH)(py)_4](ClO_4)_2$ (5): ORTEP drawings of **5** are shown in Fig. 6 together with the atom numbering scheme. Selected bond distances and angles are given in Table 6.

The $[Ni_2(L^2)(OH)(py)_4]^{2+}$ cation has a nearly coplanar μ-hydroxo-μ-phenolato-dinickel(II) core in a Ni···Ni separation of 3.156 Å. Pyridine molecules occupy the axial sites of Ni affording a six-coordinate geometry about each metal. The Ni(1)-to-donor bond distances range from 2.018 to 2.192 Å and the Ni(2)-to-donor bond distances range from 2.001 to 2.192 Å. The Ni(1)–O(1)–Ni(2) and the Ni(1)–O(2)–Ni(2) angles are 99.6° and 103.5°, respectively. The pyridine molecules attached to the axial sites of Ni(1) and Ni(2) are stacked in an average ring–ring separation of 3.51 Å.

The ligands $(L^1)^-$ and $(L^2)^-$ have a similar framework but

Table 6. Selected Bond Distances and Angles of **5**

Bond distances/Å			
Ni(1)–O(1)	2.055(2)	Ni(1)–O(2)	2.018(4)
Ni(1)–N(1)	2.041(5)	Ni(1)–N(2)	2.133(3)
Ni(1)–N(5)	2.156(4)	Ni(1)–N(6)	2.192(5)
Ni(2)–O(1)	2.077(5)	Ni(2)–O(2)	2.001(2)
Ni(2)–N(3)	2.022(3)	Ni(2)–N(4)	2.148(5)
Ni(2)–N(7)	2.167(5)	Ni(2)–N(8)	2.192(4)
Ni(1)···Ni(2)	3.156(10)		
Bond angles/°			
Ni(1)–O(1)–Ni(2)	99.6(2)	Ni(1)–O(2)–Ni(2)	103.5(2)
O(1)–Ni(1)–O(2)	78.5(1)	O(1)–Ni(1)–N(1)	88.8(1)
O(1)–Ni(1)–N(2)	178.5(1)	O(1)–Ni(1)–N(5)	93.8(1)
O(1)–Ni(1)–N(6)	93.5(1)	O(2)–Ni(1)–N(1)	167.1(1)
O(2)–Ni(1)–N(2)	100.0(1)	O(2)–Ni(1)–N(5)	91.8(2)
O(2)–Ni(1)–N(6)	89.9(2)	N(1)–Ni(1)–N(2)	92.7(1)
N(1)–Ni(1)–N(5)	91.0(2)	N(1)–Ni(1)–N(6)	88.9(2)
N(2)–Ni(1)–N(5)	86.2(1)	N(2)–Ni(1)–N(6)	86.5(1)
N(5)–Ni(1)–N(6)	172.7(1)	O(1)–Ni(2)–O(2)	78.3(1)
O(1)–Ni(2)–N(3)	88.9(1)	O(1)–Ni(2)–N(4)	178.0(1)
O(1)–Ni(2)–N(7)	93.9(2)	O(1)–Ni(2)–N(8)	90.9(2)
O(2)–Ni(2)–N(3)	166.9(1)	O(2)–Ni(2)–N(4)	99.8(1)
O(2)–Ni(2)–N(7)	92.6(1)	O(2)–Ni(2)–N(8)	89.5(1)
N(3)–Ni(2)–N(4)	93.0(1)	N(3)–Ni(2)–N(7)	91.3(1)
N(3)–Ni(2)–N(8)	87.6(1)	N(4)–Ni(2)–N(7)	86.5(2)
N(4)–Ni(2)–N(8)	175.0(1)	N(7)–Ni(2)–N(8)	175.0(1)

differ from each other in the terminal chelating residue of two pendant arms: (2-dimethylaminoethyl)imino for $(L^1)^-$ and (2-pyridylethyl)imino for $(L^2)^-$. The X-ray structural studies for $[Zn_2(L^1)(OH)(py)_2](ClO_4)_2 \cdot Pr^2OH$ (**1**·Pr^2OH), $[Zn_2(L^2)(OH)(py)_3](ClO_4)_2 \cdot 0.5Pr^2OH$ (**2**·0.5Pr^2OH), $[Ni_2(L^1)(OH)(py)_2](ClO_4)_2 \cdot py$ (**4**·py), and $[Ni_2(L^2)(OH)(py)_4](ClO_4)_2$ (**5**) reveal distinct dinuclear core structures effected by the terminal chelating residues. The ligand $(L^1)^-$ affords a non-coplanar μ-hydroxo-μ-phenolato dinuclear core for **1** and **4** (Figs. 2 and 4), owing to a significant strain arising from the five-membered chelate ring formed with the terminal residue. Each metal (Zn or Ni) has a distorted square-pyramidal geometry together with a pyridine molecule. This must be a favored structure for **1** since Zn(II) prefers five-coordination to six-coordination. Ni(II) generally prefers six-coordination in the absence of any constraint from the ligand used, but **4** retains the distorted square-pyramidal geometry about Ni in pyridine as discussed later. This fact indicates the rigidness of the dinuclear core effected by the constraint from $(L^1)^-$. The ligand $(L^2)^-$ affords a nearly coplanar μ-hydroxo-μ-phenolato dinuclear core for **2** and **5** (Figs. 3 and 5). Evidently, the dinuclear core has little strain owing to the 6-membered chelate ring formed with the terminal residue. In the structure of **2**·0.5Pr^2OH, one Zn has a square-pyramidal geometry with further coordination of pyridine (Zn–N distance: 2.098(5) Å). The other Zn has a six-coordinate geometry together with two pyridine molecules, but this structure is not necessarily favored judging from the long Zn–N(pyridine) distances (2.339(5) and 2.259(5) Å). Each Ni in **5** has a favored six-coordinate structure with two pyridine molecules at the apical sites.

Physicochemical Properties. All the complexes show a sharp IR band at 3620–3570 cm^{-1} characteristic of the ν(O–H) vibration of a bridging hydroxide group.[19,20] Complexes **1**, **2**, **4**, and **5** show the ν(C=N) vibration of the azomethine group at 1638–1656 cm^{-1}. The ν_3 mode of perchlorate group at ~1100 cm^{-1} shows no splitting in all the complexes, in accord with ionic nature of the perchlorate ion.

Complexes **1**–**3** are diamagnetic. Effective magnetic moments of $[Ni_2(L^1)(OH)(py)_2](ClO_4)_2$ (**4**) and $[Ni_2(L^2)(OH)(py)_4](ClO_4)_2$ (**5**) at room temperature are 2.84 and 2.92 μ_B (per Ni), respectively, and the moments decreased with decreasing temperature to 0.42 and 0.28 μ_B at 2 K, respectively (Fig. 7). Evidently an antiferromagnetic interaction operates between each pair of nickel ions. Each χ_M vs T curve shows a slight increase at low temperature, suggesting a contamination of a small amount of a paramagnetic impurity. The mag-

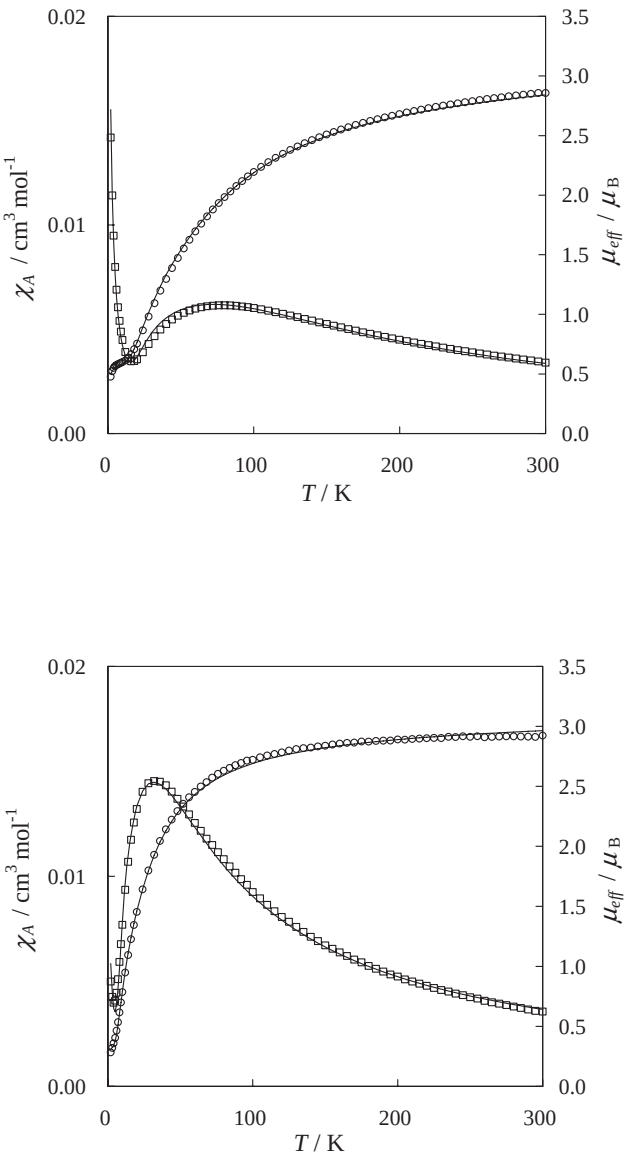

Fig. 7. Temperature-variations of magnetic susceptibility and magnetic moment (per Ni) of $[Ni_2(L^1)(OH)(py)_4](ClO_4)_2$ (**4**) (top) and $[Ni_2(L^2)(OH)(py)_2](ClO_4)_2$ (**5**) (bottom).

netic susceptibility expression of the ($S_1 = 1$)–($S_2 = 1$) system based on the isotropic Heisenberg model ($\boldsymbol{H} = -2JS_1S_2$) is given as follows:

$$\chi_A = (1-\rho)\{Ng^2\beta^2/k(T-\theta)\} \times [5 + \exp(-4J/kT)]/[5 + 3\exp(-4J/kT) + \exp(-6J/kT)] + \rho \times (g^2/4T) + N\alpha, \quad (1)$$

where ρ is the fraction of paramagnetic impurity and other symbols have their usual meanings. Magnetic properties of **4** and **5** can be well simulated by Eq. 1 as shown by the solid curves in Fig. 7. The best-fit parameters obtained are $J = -27.7$ cm^{-1}, $g = 2.15$, $\theta = -0.8$ K, $N\alpha = 400 \times 10^{-6}$ cm^3 mol^{-1}, and $\rho = 0.085$ for **4** and $J = -10.8$ cm^{-1}, $g = 2.14$, $\theta = -1.0$ K, $N\alpha = 120 \times 10^{-6}$ cm^3 mol^{-1}, and $\rho = 0.017$ for **5**. Thus, complex **4** exhibits a stronger antiferromagnetic interaction than **5**. This may be explained by the short Ni···Ni separation in **4** (3.069 Å) relative to the Ni···Ni separation in **5** (3.156 Å).

The room-temperature magnetic moment of $[Ni(L^1)(OH)H_2O](ClO_4)_2$ (**4′**) is 2.84 μ_B per molecule and the moment is essentially independent of temperature. Evidently, **4′** is a mixed-spin complex with one paramagnetic Ni(II) ion and one diamagnetic Ni(II) ion. A dinuclear core consisting of a planar Ni(II) and a square-pyramidal Ni(II) with a water molecule at the axial site can be deduced for this complex.

Molar conductance values of **1**–**5** in DMSO (55–61 S cm^2 mol^{-1}) are typical of 2:1 electrolytes in this solvent.[21] $[Zn_2(L^1)(OH)(py)_2](ClO_4)_2$ (**1**) and $[Zn_2(L^2)(OH)(py)_3](ClO_4)_2$ (**2**) each have an intense band at 390 nm, which is associated with the π–π^* transition of the azomethine linkage.[22,23] $[Zn_2(L^3)(OH)](ClO_4)_2$ (**3**) has a moderate absorption band at 307 nm. A green pyridine solution of $[Ni_2(L^1)(OH)(py)_2](ClO_4)_2$ (**4**) shows absorption bands at 402, 624, 920, and ~1400 nm (see Fig. 8). The spectral feature indicates a square-pyramidal geometry about Ni(II)[24,25] in harmony with the X-ray structural result for **4**·py. Notably, a DMSO solution of **4** assumes a reddish color and its spectrum is characterized by a distinct shoulder at ~490 nm along with d–d bands at 900 and ~1350 nm. This absorption spectrum resembles the reflectance spectrum of $[Ni_2(L^1)(OH)H_2O]](ClO_4)_2$ (**4′**) with bands at 480, 840, and 1300 nm. This fact means that **4** forms a mixed-spin species $[Ni_2(L^3)(OH)(dmso)]^{2+}$ in DMSO. It is known that Ni(II) has a high affinity for pyridine relative to DMSO.[26]

$[Ni_2(L^2)(OH)(py)_4](ClO_4)_2$ (**5**) in pyridine shows absorption bands at 583 and 990 nm in addition to the π–π^* transition of the azomethine group at 403 nm. The spectrum indicates a pseudo octahedral geometry about each Ni(II).[24] The spectrum of **5** in DMSO, on the other hand, has absorption bands at 400, 593, 905, and 1350 nm, indicating a square-pyramidal surrounding about each Ni. That is, complex **5** exists as $[Ni_2(L^2)(OH)(dmso)_2]^{2+}$ in DMSO.

From preliminary studies, we have noticed that the dinuclear zinc complexes (**1**, **2**, and **3**) cannot hydrolyze di(*p*-nitrophenyl) phosphate (DNP^-) into mono(*p*-nitrophenyl) phosphate, whereas the dinuclear Ni complexes (**4** and **5**) facilitate the hydrolysis of DNP^-.[27] The phosphodiesterase-like function of **4** and **5** will be reported elsewhere.

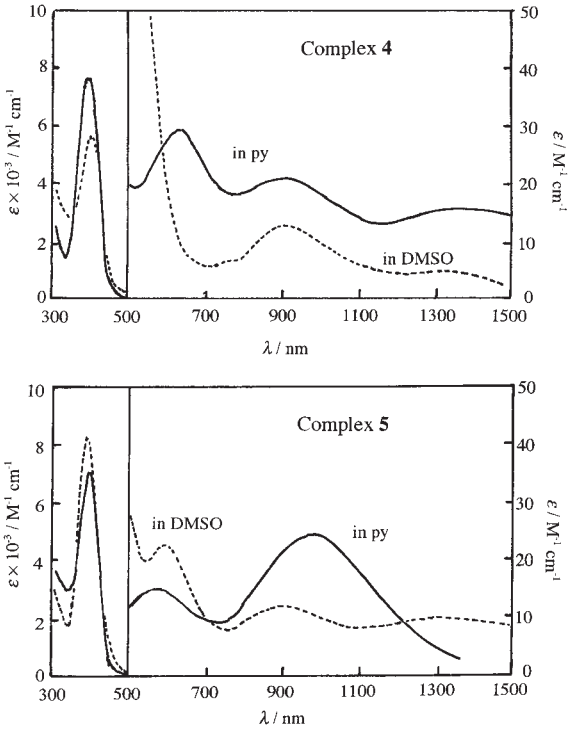

Fig. 8. Electronic absorption spectra of $[Ni_2(L^1)(OH)(py)_4](ClO_4)_2$ (**4**) (top) and $[Ni_2(L^2)(OH)(py)_2](ClO_4)_2$ (**5**) (bottom) in pyridine and DMSO.

This work was supported by a Grant-in-Aid for Scientific Research (No. 07454178) from the Ministry of Education, Culture, Sports, Science, and Technology.

References

1 D. E. Fenton and H. Ōkawa, "Perspectives on Bioinorganic Chemistry," JAI Press, London (1993), Vol. 2, p. 81.

2 E. E. Kim and H. W. Wyckoff, *J. Mol. Biol.*, **218**, 449 (1991).

3 E. Hough, L. K. Hansen, B. Birkness, K. Jynge, S. Hansen, A. Hardvik, C. Little, E. J. Dodson, and Z. Derewenda, *Nature*, **338**, 357 (1989).

4 A. Lahm, S. Volbeda, F. Sakijama, and D. Suck, *J. Mol. Biol.*, **215**, 207 (1990).

5 J. L. Vanhooke, M. M. Benning, F. M. Raushel, and H. M. Holden, *Biochemistry*, **35**, 6020 (1996).

6 N. Strater, T. Klabunde, P. Tucker, H. Witzel, and B. Krebs, *Science*, **268**, 1489 (1995).

7 S. K. Burley, R. R. David, R. M. Sweet, A. Yaylor, and W. N. Lipscomb, *J. Mol. Biol.*, **224**, 113 (1992).

8 C. R. Kissinger, H. E. Parge, D. R. Knighton, C. T. Lewis, L. A. Pelletier, A. Tempczyk, V. J. Kalish, K. D. Tucker, R. E. Showalter, E. W. Moomaw, L. N. Gastinel, N. Habuka, X. Chen, F. Maldonado, J. E. Barker, R. Bacquet, and E. Villafranca, *Nature*, **378**, 641 (1995).

9 M. P. Engloff, P. T. W. Cohen, P. Reinemer, and D. Barford, *J. Mol. Biol.*, **254**, 942 (1995).

10 J. Goldberg, H. Huang, Y. Kwon, P. Greengard, A. C. Nairn, and J. Kuriyan, *Nature*, **376**, 745 (1995).

11 A. K. Das, N. R. Helps, P. T. W. Cohen, and D. Barford, *EMBO J.*, **15**, 6798 (1996).

12 Z. F. Kanyo, L. R. Scolnick, D. E. Ash, and D. W. Christianson, *Nature*, **383**, 554 (1996).
13 E. Jabri, M. B. Carr, R. P. Hausinger, and P. A. Karplus, *Science*, **268**, 998 (1995).
14 D. A. Denton and H. Suschitzky, *J. Chem. Soc.*, **1963**, 4741.
15 M. Suzuki, H. Kanatomi, and I. Murase, *Chem. Lett.*, **1981**, 1745.
16 "teXsan," Molecular Structure Corporation, Houston, TX (1985 & 1999).
17 C. K. Johnson, Report 3794, Oak Ridge National Laboratory, Oak Ridge, TN (1965).
18 A. W. Addison, T. N. Rao, J. Reedaijk, J. V. Rijn, and G. C. Verschoor, *J. Chem. Soc., Dalton Trans.*, **1984**, 1349.
19 K. Motoda, H. Sakiyama, N. Matsumoto, H. Ōkawa, and D. E. Fenton, *J. Chem. Soc., Dalton Trans.*, **1995**, 3419.
20 L. Borer, L. Thalken, C. Cecarelli, M. Glick, J. H. Zhang, and W. M. Reiff, *Inorg. Chem.*, **22**, 1719 (1983).
21 W. J. Geary, *Coord. Chem. Rev.*, **7**, 81 (1971).
22 B. Bosnich, *J. Am. Chem. Soc.*, **90**, 627 (1968).
23 R. S. Downing and F. L. Urbach, *J. Am. Chem. Soc.*, **91**, 5977 (1969).
24 L. Sacconi, *Coord. Chem. Rev.*, **1**, 192 (1966).
25 L. Sacconi and I. Bertini, *J. Am. Chem. Soc.*, **88**, 5180 (1966).
26 H. Ōkawa, Y. Aratake, K. Motoda, M. Ohba, H. Sakiyama, and N. Matsumoto, *Supramol. Chem.*, **6**, 293 (1996).
27 K. Matsufuji, Master Thesis, Faculty of Science, Kyushu University (2003).